INHOMOGENITY OF LASER-DRIVEN TECHNOLOGICAL PROCESSES I. BEAM RELATED INHOMOGENITIES

S. Lugomer
Ruđer Bošković Institute, Zagreb, Croatia

Keywords: laser-driven technological processes, process inhomogenity, laser beam inhomogenity, inhomogene tempreatures, pressure fields, material surfaces, laser material deposition, laser chemical reactions, metal surfaces, semiconductor surface, laser treatments, laser glazing, beam-plasma

Abstract: Inhomogenity of laser-driven technological processes caused by inhomogenity of the laser beam is considered. Inhomogeneous beam induces the inhomogeneous temperature and the pressure fields on the material surface, thus dividing it into domains of the solid response, liquid response, and of the vapor/liquid response regime. The set of the gradient pairs $\Delta T^{\prime}_{\perp,\parallel}$ $\Delta P^{\prime}_{\perp,\parallel}$ give rise of 16 possible subdomains (basins) everyone of which is origin of characteristic dynamics. Depending on a dominant gradient pair combination, a number of physical phenomena is derived. They may simultaneously appear in various basins of the interaction space, generated in the single shot.

Inhomogenost laserski-iniciranih tehnoloških procesa

Ključne besede: procesi tehnološki laserski, nehomogenost procesov, nehomogenost žarkov laserskih, temperature nehomogene, polja tlakov, površine materialov, nanašanje materialov lasersko, reakcije kemične laserske, površine kovin, površine polprevodnikov, postopki laserski, loščenje lasersko, žarki plazemski

Sažetak: Razmatrana je nehomogenost laserski iniciranih tehnoloških procesa, uzrokovana nehomogenošću laserskog snopa. Nehomogenost snopa indicira nehomogeno polje, pritiska i tamperature na površini materiala i tako generira bazene različitih responsa režima: režim solida, tekućina i režim karakterističan za prijelaz tekućina/para. Skup gradijentnih parova $\Delta T^{\prime}_{\perp,\parallel}$ $\Delta P^{\prime}_{\perp,\parallel}$ daje 16 mogućih subdomena (bazena) od kojih svaki ima drukčiju dinamiku. Ovisno o dominantnoj kombinaciji gradijentnih parova, moguće je dobiti niz fizikalnih fenomena. Oni se mogu simultano pojavljivati u različitim bazenima interakcijskog prostora, generirani jednim jedinim laserskim pulsom.

Introduction

This paper deals with very common phenomena appearing in many (if not all) laser-driven technological processes, i.e. the process inhomogenities. They have been observed in:

- laser material deposition
- laser chemical reactions on the surface of metals and semiconductors
- laser treatment of metal surfaces
- laser glazing,

on both, thin films and plates. They are important for the surface processing technology on the microscale but in the engineering of the surface properties, surface protection, alloying and cladding on the macro- scale as well. These inhomogenities originate from laser-material (L-M) interaction, depending on the wavelength-scale (λ-scale), on the power- scale (P-scale), and the pulse duration (τ-scale), i.e. on the "beam related scales". Besides, they depend on the experimental conditions like the beam size, and the scan velocity, but also on the type of the material. Inhomogenities may be characterized with respect to "regime" of the surface response, determined by the maximal temperature reached in the L-M interaction.[1]

For the L-M interaction with $T_S < T_{melting}$, i.e. for the "solid response regime", the inhomogenity may appear in the form of plastic and superplastic deformations sometimes accompanied with various kinds of cracks.[1]

For the L-M interaction with $T \geq T_{melting}$, i.e. for the "liquid response regime", the inhomogenities may appear as 2D turbulent flow, vortices, viscous fingering, 1D and/or 2D supersonic jets, the convection phenomena etc..

For the L-M interactions exceeding T_B, i.e. in the presence of the surface ablation, or in the "vapor/liquid response regime", the inhomogenities may appear in the form of Rayleigh-Taylor R-T instabilities, various kinds of craters, transition from planar to nonplanar ablation etc.[1]

Here we should mention a very complex case of the high-power laser-metal interactions in the gaseous atmospheres when (in addition to the above types of response), one finds the surface chemical reactions. The inhomogenity appears in the form of different reaction rates, different types of reaction and consequently

of different composition on various places of the interaction space. In the high-power pulsed L-M interactions, the inhomogenity is observed as a fingerprint of the surface dynamics frozen in the interaction space. The pattern is of the complex nature, consisting of individual separated basins of the surface response dynamics.

Inhomogenities in the high-power L-M interactions have been mentioned in the literature many times. Their origins have been very seldom discussed, and in general, they are not well understood. Interest for these interactions was recently well increased because of their importance in the laser-driven technological processes on one side, and because of purely fundamental reasons on the other side. Up to now there is no systematic overview of inhomogeneous L-M interactions, and of physical phenomena simultaneously taking place in the interaction space.

This paper, on the phenomenological basis, and in a scatchy way, connects a number of these phenomena with their source in the laser beam.

Origins of inhomogeneity in the L-M interactions

Inhomogeneity in the L-M interaction may be caused by two type of sources: those (i) beam related, and those (ii) material related.

The beam-related sources are:

(i) laser beam inhomogenity [2, 3, 4]

(ii) inhomogeneous beam-plasma interaction above the material surface, while the material -related sources are:

(i) ablation instability[5]

(iv) structural /compositional surface disorder.

In this paper we consider the beam-related-sources.

(i) Laser beam inhomogeneity

Laser beam inhomogenity appears in the surface multimode processing (laser transformation hardening, laser glazing, laser alloying...). Multimode processing is strongly recommended because of the "top hat" profile and optimal surface covering.[6] In such a case the first few modes are dominant, and the beam structure (in the transversal cross-section) is approximately homogeneous and constant in time.

However, in the multimode, high repetition pulsing, the laser operation may become unstable. Multimode oscillations change the beam structure and cause the intensity space-time oscillations. These phenomena belong to the class of nonlinear optics and bring the analogy with the nonequilibrium phase transitions.[2,3,4]

Spontaneous mode-mode transitions are common in nonlinear optical systems (variously called self-focusing, fillamentation or profile instability) and lead to the formation of complex spatial structures, whenever the Fresnel number F, $F = \frac{\rho_0^2}{\lambda L}$, is small, ($\rho_0$ = mirror radius, L = laser cavity length, λ = wavelength). It may be understood as the ratio between the geometric angle ρ_0/L of view of one mirror from the other, and the difractive angle λ/ρ_0.[2]

The new features leading to increasing complexity of multimode spatial patterns appear when nonaxially symmetric modes are present. They can be described as a number (and dynamical motion) of defects in the patterns (where the intensity is zero, about which the electric field phasors[7] circulate and through which the electric field changes sign.(3) Defect in the optical field can appear for only a two modes present (for example with the combination of two Hermitte-Gaussian modes of indices n, m and m, n with a phase shift of $\pi/2$). Complex patterns can appear when the number of active modes is as many as five.[3]

The study of these problems was recently intensified from a few standpoints. Theoretically, one can look for the numerical solutions of the full set of Maxwell-Bloch equations describing the multimode laser operation and analyze the results in terms of the appearance and motion of defects in the intensity patterns.[3]

Alternatively, one can start from defects in the intensity field, and make the analogy with defect-mediated turbulence, by the study of influence of the singularities on the correlation of intensity fluctuations at spatially separated points and on the existence of different temporal and length scales in the system.[3] Here we concentrate on the time scales of fluctuations equal or larger than the pulse duration, so that the instantaneous mode pattern is the actual (pulse) pattern structure.

D'Angelo at al.[3] have shown that for small values of gain, C, and small Fresnel numbers (C = 1.1, a= 0.1) the intensity patterns are radially symmetric and the total intensity is time independent.

(Parameter a is related to the Fresnel number through: $a = \frac{8}{T}\tan^{-1}\left(\frac{L\lambda F}{4\pi\rho_0^2}\right)$, where T = oscillation period and ρ_0 = mirror radius)

More than 1 mode are present in the cavity, but the intensity is stationary in time - representing the cooperative frequency looking.

Upon increasing C(C = 1.2, a = 0.1) periodic pulsations in the laser intensity appear.[3]

Further increase of C leads to the appearance of complex spatio-temporal structures, each bifurcation involves the simultaneous appearance of a new frequency in

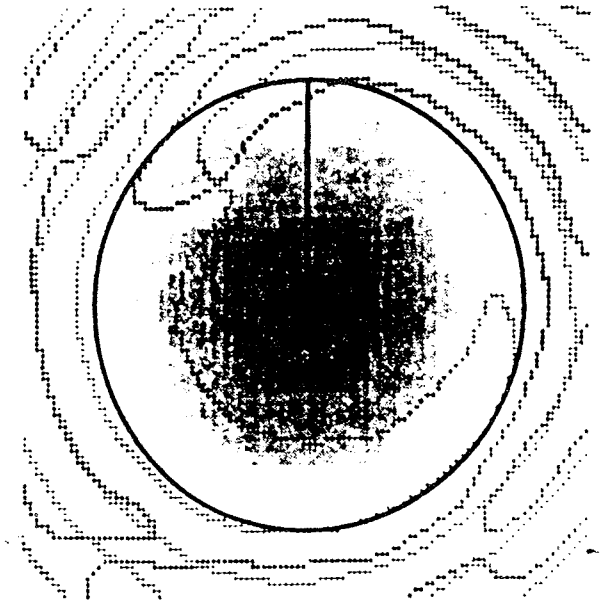

Fig. 1: Pattern a single defect of periodically pulsating intensity with for C = 2.5 and a = 0.1. Isophase and brightness plot the instantaneous intensity distribution. Darker shading corresponds to higher intensity. In this graph crossed (dotted) lines in the x-y space are the locus where the real (imaginary) part of the field vanishes. The point marked in the fixture is a topological defect. The solid circle marks the nominal boundary of the laser. $\rho = \rho_0$ (where the losses rapidly increase) while the solid line is an aid to identifying the center of the pattern $\rho = 0$. From ref. 3.

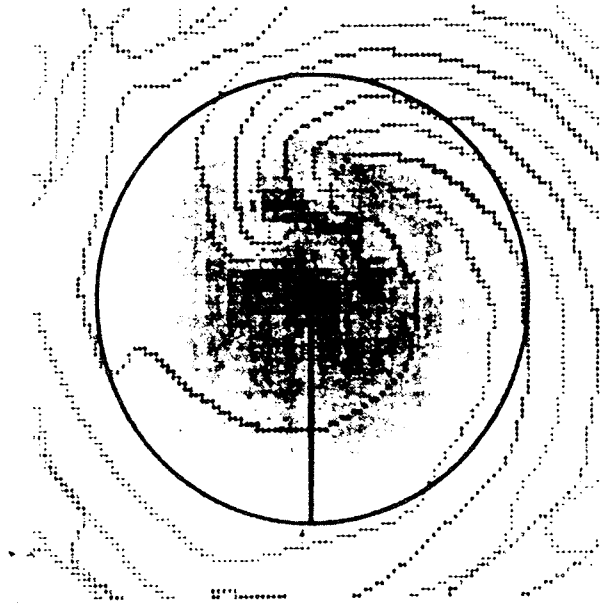

Fig. 2: Pattern of quasiperiodically pulsating intensity with two defects for C = 3.5 and a = 0.1. From ref. 3.

the intensity power spectrum and a spontaneous symmetry breaking of the spatial structure.[3]

Increasing the gain (C = 2.5, a = 0.1) the intensity becomes time dependent but the pattern at any particular time has an asymmetric profile. Oscillations of the intensity in time at each point of the pattern are periodic and are locked to the ratio 1;19.[3] The equiphase lines corresponding to this pattern show the existence of a point near the center where both real and imaginary parts of the field are zero simultaneously. This point is called "defect" in the beam structure.[3] Fig. 1. This defect can also be viewed as a phase vortex as the electric field phases have a net circulation around this point which when measured in mitts of 2π is called its topological charge. In this case the defect has a topological charge +1. Analysis of equiphase lines shows that the location of the defect is rotating around the center of the beam. This motion is in the form of a traveling wave of the type $\cos(l\phi - \omega t)$.[3]

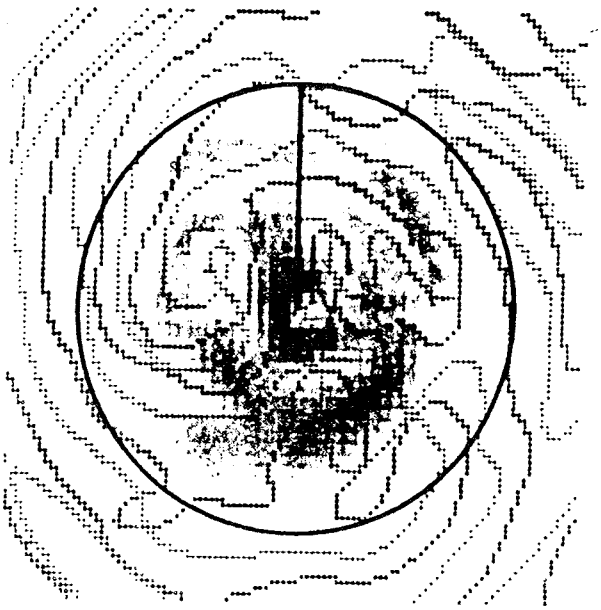

Fig. 3: Pattern with on average of 9 moving defects. Instantaneous equiphase lines showing the presence of mine defects. From ref. 3.

Increasing the gain further on (C = 3.5, a = 0.1) a more complex pattern appears. It contains two "defects" present in the beam, rotating around the center of the beam at different speeds.[3] Fig. 2.

Even more complicated patterns are obtained for C = 3.5, a = 0.4, in which many "defects" are present. In fact we get locally chaotic behaviour of intensity. Fig. 3. This pattern has (in average) nine defects of various topological charge. The number of defects is not constant, as pairs of opposite topological charge can annihilate and pairs can be also created.[3] These phenomena were recently discussed by Arecchi[2]. The transverse (x, y) intensity pattern and its autocorrelation function (right) are shown. Fig. 4a. For low F (F = 5) one single mode at the time oscillates and the wavefront is wholly correlated, and the correlation length ξ is of the some order or the cross lie D of the beam.(2) Fig. 4b. For high F (F = 70) many modes oscillates simultaneously yielding a speckle-like pattern (C), whose correlation length ξ is very small. Fig. 4c.

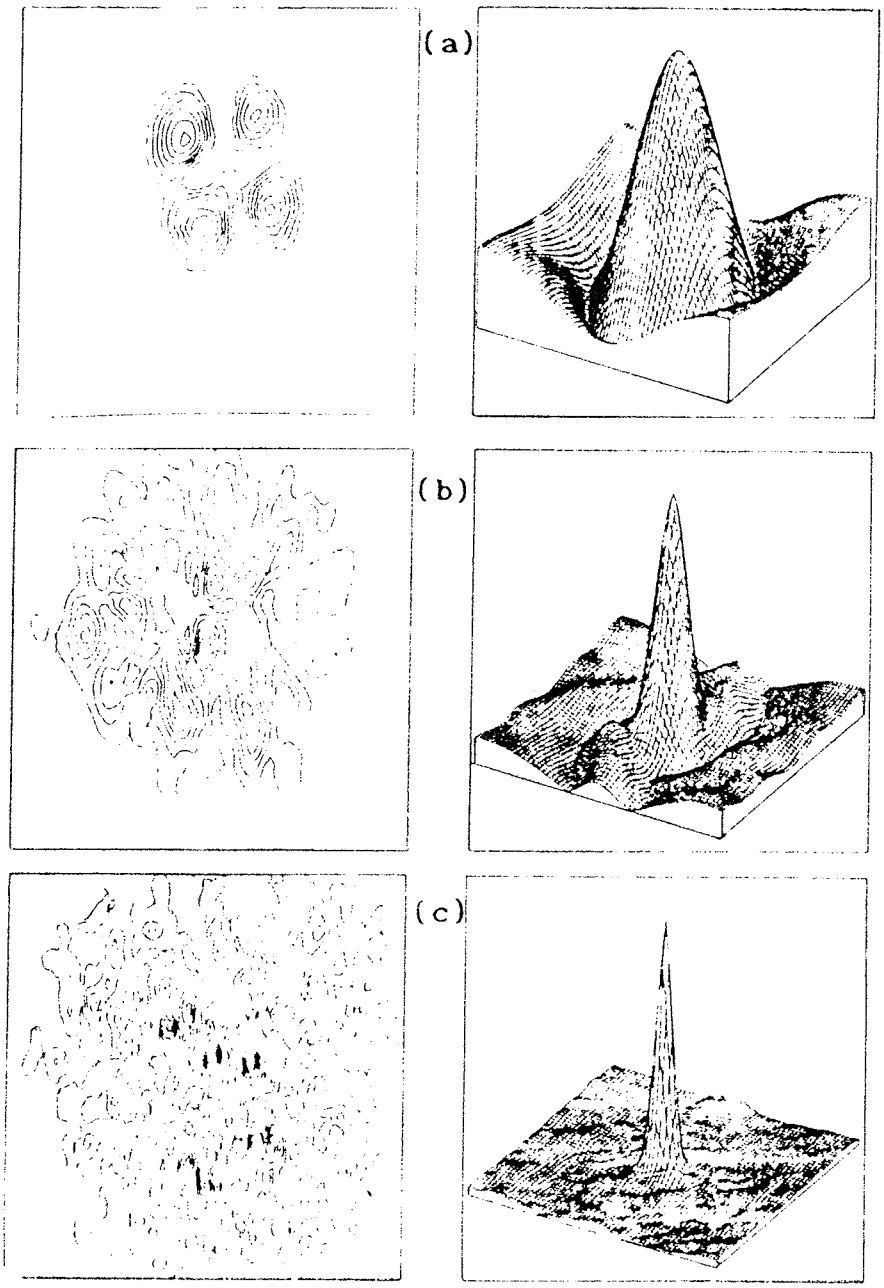

Fig. 4: *Intensity distribution on the wavefront (left) and space autocorrelation function (right) for increasing Fresnel number. (a) F = 5, one single mode at a time is present, ratio between coherence length ξ and frame size D is ξ/D = 1. (b) F = 20, ξ/D = 0.25. (c) F = 70, ξ/D = 0.1. From ref. 2.*

The low-limit F, corresponds to a periodic alternation of a few modes of the diffraction limit propagation followed by a dark period.[2] Technically, transition to the unstable multimode laser operation is sensitive on a number of operating parameters and conditions. It is sensitive on the variation of the laser pump profile (which adds spontaneous emission noise) and affects the beam intensity structure.

It is sensitive on the variation on the cavity loses (which may be important for the larger cavity radius). It is sensitive on the environmental influence on laser operation through the temperature oscillations, vibrations etc. which may influence the resonator parameters.

It is sensitive on the gain variation, which may appear if the processing conditions put the requirement for the high power at high pulse representation rate, etc.

Finally, it is sensitive on the back reflection of the beam from the metal surface. Radiation traveling in opposite direction enters resonator under small angle - and changes population emission. (The effect is equivalent to the

variation of the Fresnel number F and appearance of the asymmetric gain in the cavity.)

Whenever we have multimode laser operation every mode is a Hermitte- Gaussian (HG) or Laguerr-Gaussian (LG) function. The set of all these functions represent the topological, multidimensional space X, i.e.

$$x_i = A_{m,n} \qquad m,n = 0,1,2$$

$$\text{and } X \supseteq \{x_1, x_2, x_i \ldots\}, \qquad (1)$$

where $A_{m,n}$ stays for the HG or LG functions. Projection of the space X into the physical space, represents the optical intensity field I(x,y), for which we can simply write

$$I(x, y) \propto \sum_{m,n} A_{m,n}(x,y) \qquad (2)$$

(ii) Inhomogeneous beam-plasma interaction

At the high laser-power densities exceeding 10^8 W/cm^2 applied for the laser shock hardening or similar processes, generation of the vapor/plasma cloud above the material surface is the basic phenomenon. The plasma cloud is created by the leading edge of the pulse, while the rest of the pulse is partially absorbed in the cloud, and partially transmitted to the metal surface. Plasma density oscillations (as observed for the high power Nd:YAG and CO_2 lasers) are the common processes. In addition, arise of the plasma turbulence, inhomogeneous pair recombination etc., may cause the inhomogeneous beam scattering, absorption, or other complex photonic phenomena. Consequently, the surface will be (inhomogeneously) irradiated as to be stochastically screened. It receives less energy below the highly absorption regions of the plasma cloud, and more energy below the nonabsorptive regions.

In short, the homogeneous single mode laser beam, passing through the inhomogeneous material (plasma) cloud becomes inhomogeneous, just before it reaches the material surface. In this case the scattering functions $\alpha_{m,n}$ also give rise of multidimensional space X, whose projection into the real space gives the beam intensity I(x,y).

Generation of the Stochastic fields

The L-M interaction represents the mapping of the vector space X (beam related space) into the vector spaces Y and Z (material related spaces):

$$I_1 : X \dashrightarrow Y$$
$$I_2 : X \dashrightarrow Z. \qquad (3)$$

Supposing that the L-M interaction occurs in very short time so that dissipation processes are not significant, both imaging processes I_1 and I_2 represent nearly isomorphous mapping of X into Y and Z spaces. It means that the vector fields may be expressed by the

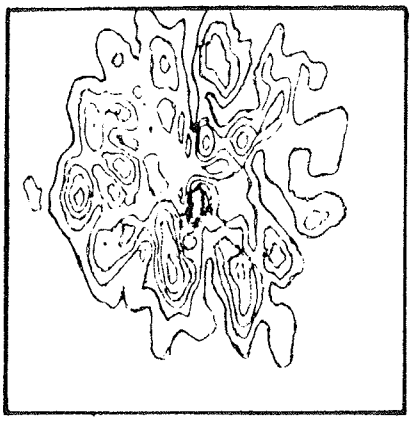

A

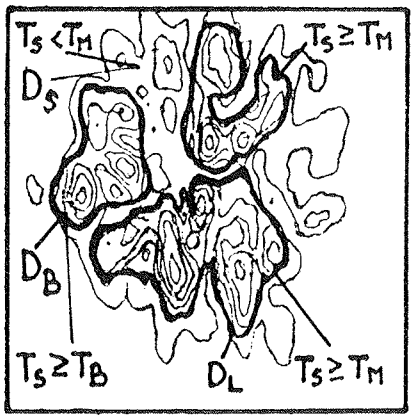

B

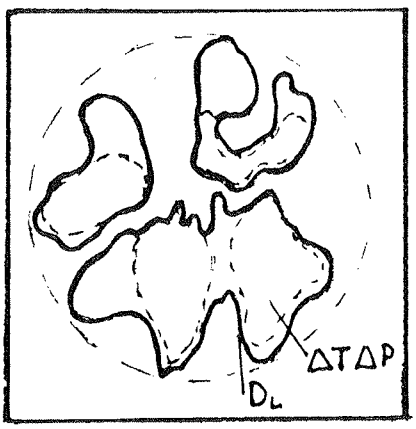

C

Fig. 5: Mapping process which transforms the stochastic optical intensity field into the stochastic temperature intensity field. (Schematically).
a) inhomogeneous optical intensity
b) inhomogeneous temperature intensity on the surface Dark lines are convolutes of the domains $D(T < T_M)$, $D_L(T > T_M)$ and $D_B(T > T_B)$
c) Definition of subdomains (dashed lines) inside domains D_S, D_S and D_B.

representing solution of diffussion equation (Bessel functions). Projection of the X space into the physical space represents the optical intensity, while the projections of Y and Z spaces, represent the temperature intensity and the pressure intensity, respectively (induced by the laser on the material surface). In this interaction the maps of the temperature and the pressure fields are similar to map of the optical field. (This, in fact, is well known for the lowest order mode TEM_{00}). For the long pulses, and for the significant role of thermal diffusivity, convection, etc. the mapps in Y and Z are very different from the mapps in X becouse of dissipation processes. The mapping process representing the L-M interaction is schematically given in Fig. 5. The stochastic optical intensity field is given in Fig. 5a. Nearly isomorphous mapp of the temperature field is given in Fig. 5b. The temperature field is obviously the stochastic field in which contours (Fig. 5b) represent the isotherms.

Further analysis of L-M interaction requires some characterization of this field to be introduced.

In the next step one can make the convolution of the isothermal curves by taking the convolute equal to T_M (melting temperature of the system), and T_B (boiling temperature). Thus, all these isothermal curves will be convoluted into 3 groups; one, which convolutes all isothermal curves $T_S \geq T_B$, one which convolutes all the curves $T_M \leq T_S < T_B$, and the third one in which stay all the isotherms outside the above two, i.e. those for which $T_S < T_M$. Fig. 5b.

Therefore, comparing the temperature intensity with the system transformation temperatures the three response regimes can be identified: the solid one ($T_S < T_M$), the liquid one ($T_S > T_M$) and the boiling one ($T_S < T_B$) or the vapor/liquid. The region inside any of the above convolutes is called a domain **D**. The interaction space therefore, consists of domains which may be of the solid, liquid or the vapor/liquid type. Further characterization of domains is based on the directional first-derivative operators. The directional operation yield a good localization of the intensity changes.

Following this idea we concentrate on the first-directional derivatives of stochastic temperature and pressure fields, ΔT and ΔP, inside the domain **D**. A part of domain in which ΔT and ΔP change only slightly from a given value (in module and direction), is called a subdomain D. A domain space D is supposed to consists of subdomains represented by the pair of ΔT, ΔP gradients. Assuming that subdomain has the coordinate R, the local gradients will be denoted by $\Delta T(R)$, $\Delta P(R)$. Fig. 5d. Therefore, any point in the interaction space satisfies: $(x,y) \in D \subseteq \mathbf{D}$, with

$$[\Delta t\,(R), \Delta P(R)] \in D. \qquad (4)$$

Local gradient field classification

Representation of subdomains can be made more precise by decomposing the thermal gradient field with respect to the surface, into two components:

$$\Delta T(R) = \Delta T_{\perp}(R) + \Delta T_{\parallel}(R) \qquad (5)$$

as well as the pressure gradient field:

$$\Delta P(R) = \Delta P_{\perp}(R) + \Delta P_{\parallel}(R). \qquad (6)$$

Considering the subdomain with the solid surface response, all the possible cases characterizing any subdomain may be represented by the combination of gradient pairs: $\Delta T_{\perp}(R)\ \Delta P_{\perp}(R)$; $\Delta T_{\parallel}(R)\ \Delta P_{\parallel}(R)$; $\Delta T_{\perp}(R)\ \Delta P_{\parallel}(R)$ and $\Delta T_{\parallel}(R)\ \Delta P_{\perp}(R)$.

The situation is more complex for the subdomain with the liquid response regime. However, the most complex and most general case occurs for the subdomain with the surface ablation, i.e. for the vapor/liquid interface dynamics. In the case of ablative interaction, one should take into account the fact that vertical temperature and pressure gradients $\Delta T_{\perp}(R)$ and $\Delta P_{\perp}(R)$, have either (+) or (-) sign.

The (+) sign will be attributed to the case when the temperature is the highest on the surface and decreases toward the metal interior. The negative (-) sign will be attributed to the case when the highest temperature is below the surface and the lowest on the surface.

The negative vertical temperature gradients $\Delta T_{\perp}^{-}(R)$ may appear because of subsurface superheating in the evaporation of the target. The surface is being cooled by the latent heat of evaporation, while the finite amount of laser energy is deposited within a certain depth from the surface of the target. This depth is characterized by the inverse of the absorption coefficient of the target for the incident laser beam. In contrast to the surface latent heat cooling mechanism, the only cooling mechanism inside the target is the conduction of heat into the bulk.(8) This results in internal temperatures being higher than the evaporating surface temperature, thus generating negative temperature gradient, $\Delta T_{\perp}^{-}(R)$.

The degree of superheating or $|\Delta T_{\perp}^{-}|$ module is dependent on the pulse duration τ and was observed on the nanosec. time scale. As a pulse duration is decreased to about 10 ns, the degree of superheating shows almost linear increase[8]. As the pulse duration increase for example above 120 ns, the superheating effects **vanish, thus meaning that** $\Delta T_{\perp}^{-}$ is transferred into the positive one, i.e. $\Delta T_{\perp}^{+}$. This is a direct influence of the beam parameters (P, τ) on the structure of the thermal gradient fields.

The pressure field in the above case especially $\Delta P_{\perp}(R)$ component is also reversed. Namely, the inverse thermal gradient $\Delta T_{\perp}^{-}(R)$ causes (because of the subsurface

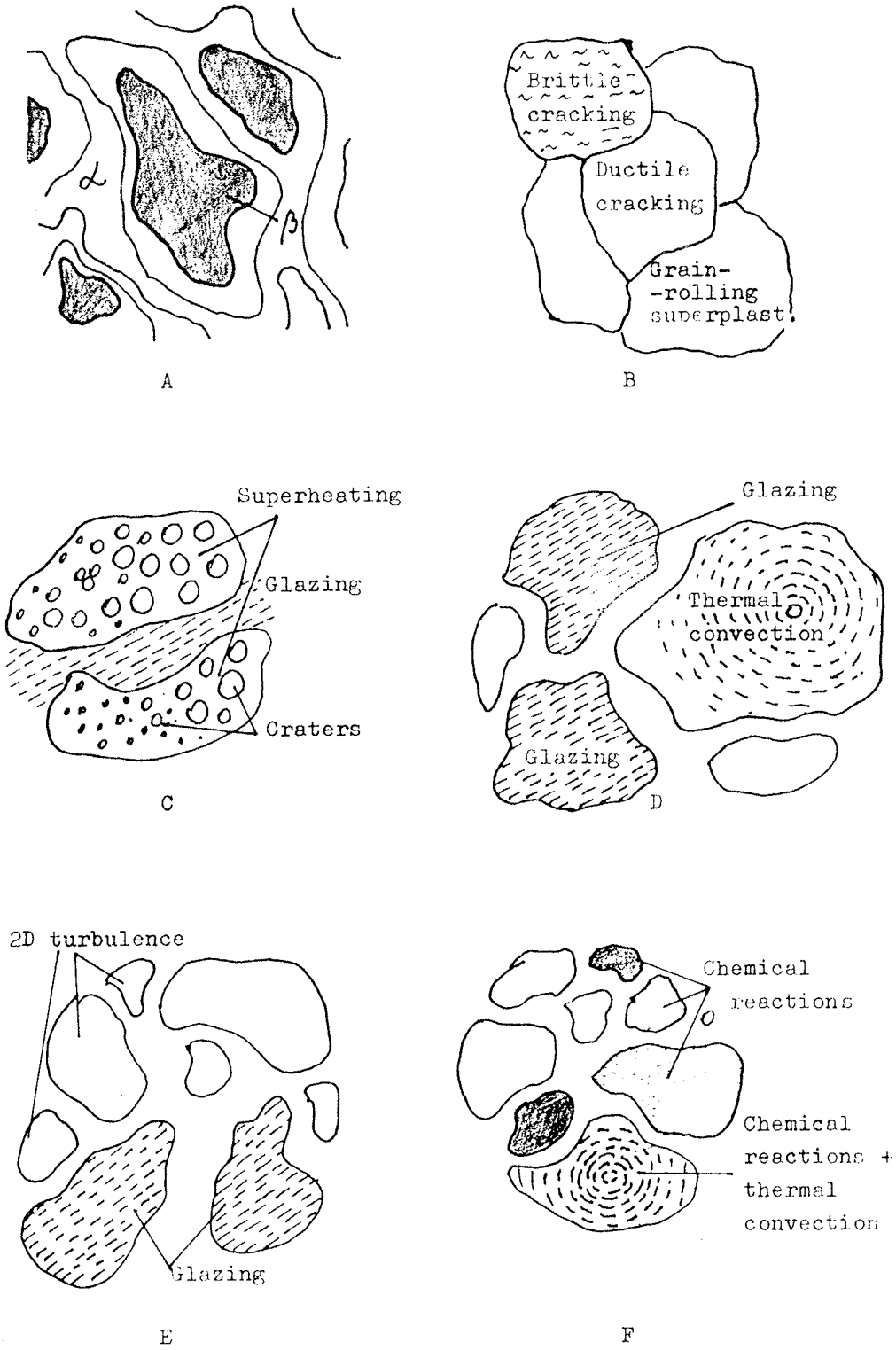

Fig. 6: *Schematic illustration of the inhomogeneous L-M interaction:*
a) in the case of inhomogeneous solid-solid phase transformation on the surface of composite materials (alloys).
b) in the case of inhomogeneous appearance of plastic and superplastic basins, accompanied by different types of cracks
c) in the case of inhomogeneous appearance of subsurface superheating and glazing
d) in the case of inhomogeneous appearance of glazing and thermal convection
e) in the case of inhomogeneous appearance of 2D turbulence and glazing
f) in the case of inhomogeneous surface chemical reaction (in alloying/cladding) accompanied by thermal convection and glazing. (See text.)

gas phase nucleation) a strong, inverse $\Delta P_{\perp}^{-}(R)$ gradient component.

Thus, both gradients $\Delta T_{\perp}(R)$ and $\Delta P_{\perp}(R)$ may, in general, have (+) or (-) sign. For the reason of completeness one should allow (+) and (-) signs for the horizontal gradients of $\Delta T_{||}(R)$ and $\Delta P_{||}(R)$, too. (As a matter of fact the two neighbour subdomains with either $\Delta T_{\perp}^{+}(R)$ or $\Delta T_{\perp}^{-}(R)$ of different modules automatically induce the horizontal $\Delta T_{||}^{-}(R)$ or $\Delta T_{||}^{+}(R)$ gradients). The reference point for the (+) or (-) ort orientation of horizontal components is the center of the particular subdomain. In this respect (+) sign of $\Delta P_{||}(R)$and $\Delta T_{||}(R)$ will relate to the ort orientation from the center of the subdomain toward its periphery, and vice versa for the (-) components sign.

On the basis of the above gradient field notation one can realize the mathematical construction as a representation of all possible cases of the local gradient field(s) configuration, given in the TAB. I.

This representation gives a 16 subdomains with specific configuration of the process-driving fields capable to generate a number of physical phenomena in the interaction space and in the single shot.

Local field characteristics and arise of physical phenomena

Dominant components of the local gradient field initiate a specific kind of phenomena in the particular subdomain.

Since the term subdomain is more familiar with mathematical consideration, we shall use the term "basin" which is more familiar with the physical description of dynamical processes. The list of physical phenomena (which is not complete) characteristic for various basins is given in TAB. II.

In the complex pattern of inhomogeneous L-M interaction, various basins are, first identified in the micrograph. Then, they are classified according to physical phenomena on the basis of TAB. II. Finally, local field configuration is identified. This procedure should be repeated for every basin in the micrograph.

A few characteristic examples appearing on refractory metals (Ti, Ta, Mo, W), are described below, and schematically illustrated in Fig. 6.

The "solid type response" represents the case appearing in the laser- transformation hardening of composite materials. These materials may have a complex phase diagrams with transitions of solid-solid type. The L-M interaction which establishes the inhomogeneous temperature distribution may cause inhomogeneous transformation, or appearance of the small zones of phase β (or γ) inside the matrix of the α phase. Schematically, this phenomena is illustrated in Fig. 6a.

Another example of the "solid type response" was observed in the Q-switched Nd:YAG high power multipulse treatment of refractory metals, (Ti, Ta, Mo, W...) with the high degree of beam focusing (2ω = 90 μm).[9] Fig. 6b. All the basins are of the solid type response. Different types of the surface breakdown (cracking) appearing above the critical power density - were obtained in every basin. Different crack growth mechanisms and the crack organization are obtained by the specific stress field configuration and by the symmetry of defects which

TAB. I: Representation of th local gradient fields

Symbolic notation	Local field configuration
1. $\Delta T_{\perp}^{+}(R)\,\Delta P_{\perp}^{+}(R)$	↓↓
2. $\Delta T_{\perp}^{+}(R)\,\Delta P_{\perp}^{-}(R)$	↓↑
3. $\Delta T_{\perp}^{-}(R)\,\Delta P_{\perp}^{+}(R)$	↑↓
4. $\Delta T_{\perp}^{-}(R)\,\Delta P_{\perp}^{-}(R)$	↑↑
5. $\Delta T_{\perp}^{-}(R)\,\Delta P_{||}^{+}(R)$	↓→
6. $\Delta T_{\perp}^{+}(R)\,\Delta P_{||}^{-}(R)$	↓←
7. $\Delta T_{\perp}^{-}(R)\,\Delta P_{||}^{+}(R)$	↑→
8. $\Delta T_{\perp}^{-}(R)\,\Delta P_{||}^{-}(R)$	↑←
9. $\Delta T_{||}^{+}(R)\,\Delta P_{\perp}^{+}(R)$	←↓
10. $\Delta T_{||}^{+}(R)\,\Delta P_{\perp}^{-}(R)$	←↑
11. $\Delta T_{||}^{-}(R)\,\Delta P_{\perp}^{+}(R)$	→↓
12. $\Delta T_{||}^{-}(R)\,\Delta P_{\perp}^{-}(R)$	→↑
13. $\Delta T_{||}^{+}(R)\,\Delta P_{||}^{+}(R)$	←→
14. $\Delta T_{||}^{+}(R)\,\Delta P_{||}^{-}(R)$	←←
15. $\Delta T_{||}^{-}(R)\,\Delta P_{||}^{+}(R)$	→→
16. $\Delta T_{||}^{-}(R)\,\Delta P_{||}^{-}(R)$	→←

Table II: Local field representation and arrise of physical phenomena

	local field represent.	The set of material parameters taking place in physical phenomena:
	$\Delta P_{\perp}^{+-}(R)$	$\mathcal{M}_p \in \{ \varepsilon, \dot{\varepsilon}, E, k, D..\}$
		ε = strain amplitude, $\dot{\varepsilon}$ = strain rate, E = Young module, k = thermal conductivity, D = vacancy diffussion coef.
	$\Delta P_{\perp}^{+-}$	– Spallation of metal grain
	$\Delta T_{\perp}^{+}(R)\,\Delta P_{||}^{+-}(R)$	– plastic behaviour controlled by $\dot{\varepsilon} < 2$; $\Delta P_{\perp}^{+-}$ component is origin of the strong shear waves which travel in all directions because of reverberations from the sample boundaries.
		– generation of vacancies and cavitation at grain boundaries (GB); [9,10]

		– cavity aggregation at GB junctions of "triple junction" type (Y-type) generating the "wedge crack" equilateral triangular crack and "isoscales triangular" crack.(10) The other cavity aggregation centers are "twin boundary", "ledge" and the "cusp", every one generating different type of crack.
	?	– "the bull eye" structure, osberved on the surface of Cu, Al and Ta[11], not well understand.
	$\Delta T_{\perp}^{+}(R)\ \Delta P_{\parallel}^{+-}(R)$	– Superplastic behaviour controlled by $\dot{\varepsilon} < 2\ \Delta P_{\perp}^{+-}$ components generate the shear waves which deposite the stress σ on the Y-sites (triple junction sites). Assymetric loading of 3 GB of the Y-site - one compressive, one tensile and one sliding-leads to the grain rotation with cleavage appearing on the tensile GB.[12] (Paidar and Takeuchi model) symmetric loading of 3 GB of the Y-site leads to the grain rotation with uncompensed tension at the center of the Y-site, thus generating the triangular crack in the center.[12] (The model of Beere). The other types of the grain rotation seems to be also present.

TAB. II: (continued)

LIQUID RESPONSE REGIME		
	local field represent.	The set of material parameters taking place in physical phenomena:
	$\Delta P_{\perp}^{+}(R)$	$\mathcal{M}_p \in \{\nu, \gamma, k, Ra, P, N..\}$ ν = kinematic viscosity, γ= surface tension, k = thermal difussivity, Ra = Raynolds number, P = Prandtl number, N = Nusselt number.
	$\Delta T_{\perp}^{+}(R)\Delta P_{\parallel}^{+}(R)$	– hydrodynamic 2D flow
	$\Delta T_{\perp}^{+}(R)$ $\Delta P_{\parallel}^{+-}(R)$	– shear flow in the micron size regions or larger. Appearance of regular structures (regular solutions), and very irregular ones (transition to turbulence). In the high power laser-metal intreractions turbulent structures are dominant.
	$\Delta T_{\perp}^{+}(R)\ (\Delta P_{\parallel}^{+-})$	– viscous fingering (equivalent to directional solidification), caused by the horizontal thermal gradient.
	$\Delta T_{\perp}^{+}(R)$	– convection instability appearing for $R_a = \frac{v_{\perp} d}{\nu} \geq 10^3$. ($v_{\perp}$ is temperature induced vertical fluid motion, d = layer thickness). They appear as: a) regular roll structures (Benard structures for steady conditions) of circular symmetry taking form of rings. b) irregular, disturbed rings, and c) chaotic, or turbulent patterns. In many cases, especially on Ta, the convection waves were observed.[13,14] The other (mixed type, structures found on Ti seems to indicate the nonvariational principle i.e. the non- potential nature of the problem.[15]
		– Benard-Marangoni convection in the presence of surface tension γ.
	$\Delta T_{\perp}^{+}(R)\Delta P_{\parallel}^{+}(R)$	– 1D and/or 2D supersonic jets of liquid metal traversing one or more liquid basins. ($\Delta P_{\parallel}^{+}$ induces the strong $v_{\parallel}$ component).
	$\Delta T_{\perp}^{+}(R)\Delta P_{\parallel}^{+}(R)$	

TAB. II: (continued)

VAPOR/LIQUID RESPONSE REGIME		
	local field represent.	The set of material parameters taking place in physical phenomena:
		$\mathcal{M}_p \in \{\nu, \gamma, Ra, P, N, \rho, A...\}$ ν, γ, Ra, P, N = as defined before, A = Atwood number, ρ = density.
	$\Delta P_{\parallel}^{+}(R)$	– viscous fingering
	$\Delta T_{\perp}^{+}(R)\Delta P_{\perp}^{+}(R)$	– Rayleigh-Taylor instability: vertical temperature gradient $\Delta T_{\perp}^{+}$ induces strong $\Delta\rho_{\perp}^{+}$ density gradient, this generating the two layer structure with ρ_{HIGH} and ρ_{LOW}. For the laser-induced R-T instability, the ratio $A = \frac{\rho_H - \rho_L}{\rho_L + \rho_H}$, called the Atwood number ≈ 1. The two types of bubles, appearing in (+) and (-) pairs as small 2D structures, or large 3D ones were found. These structures are the scale selected.[16]
	$\Delta T_{\perp}^{-}(R)\Delta P_{\perp}^{-}(R)$	– subsurface superheating: vertical temperature gradient causes subsurface boilling, and the buble generation on the surface. The exploded bubbles leave the craters on the surface. (Gas phase expelled). In some cases, the hot liquid metal comes to the surface, where $\Delta P_{\parallel}$ causes its 2D flow. This flow is irregular, organized into the structure of "dragon" (spiral) type, which can only be obtained by mathematical construction called the Barnsley collage. (Liquid phase expelled). For the subsurface superheating which ocurs in time shorter than time for the void formation, the small metal grains or their parts are expelled from the metal interior. Very irregular craters sometimes accompanied by melting are generated. (solid phase expelled).

play the role of the organizing centers. Surface breakdown structures were separately treated and their systematization was given with respect to the level of their topological complexity.[1]

In another case relating to the "liquid type response" obtained by the Q- switched Nd-YAP laser (P = Perovskite) again on the surface of refractory metals (especially on Ta plates), a different kind of inhomogeneous response was observed. The interaction

space consists of basins showing the superheating effects in the form of craters (regular), or of hillocks (still unexploded), and of basins showing pure glazed zones.[17] Fig. 6c.

Examples of inhomogeneous "liquid type response" may appear in the laser solidification hardening based either on the

- grain size strengthened alloys
- dispersion strengthened alloys
- metastable substitutional alloys
- amorphous, or glassy alloys,

where different new phases may appear inside the matrix of the old one, in the form of localized basins.

Another class of effects appear in the pulsed CO_2 laser treatment of Ti and Ta plates in the gaseous atmospheres of N_2 or O_2 under pressure. By changing the number of pulses, power density ... various kinds of phenomena appear in the basins of the inhomogeneous response.[14] Fig. 6d, e, f. Inhomogeneous interaction on the above figures contains two or three types of physical phenomena, located in separate basins. Every of these phenomena is established under specific conditions, or the field gradient representation which can be identified on the basis of TAB. II.

Plastic behaviour with cavitation cracking is established in the basin with $T_S < T_M$ in particular with $T_S < 0.3\ T_M - 0.4\ T_M$, and $\dot{\varepsilon} < 2$. The component $\Delta T_\perp{}^+$ establishes the layer of the above temperature of the thickness d (≈ to the grain size), while $\Delta T_{||}{}^{+-}$ defines the size of the basin on the surface in which the effects take place. The driving field represent the $\Delta P_{||}{}^{+-}$ components which establish the "shear waves" and cause the cavitation based "plasticity". The cavities aggregate on the point defects like triple junctions (Y-sites) giving rise of the wedge crack, isosceles triangular and equilateral triangular crack, depending on the aggregation symmetry.[10]

Superplastic behaviour is established in the basin with $T_S < T_M$, in particular with $0.7\ T_M < T_S - 0.9\ T_M$, and with $\dot{\varepsilon} \geq 2$. The component $\Delta T_\perp{}^+$ establishes the layer of the above temperature, and $\Delta T_{||}{}^{+-}$ establishes the (surface size) of the basin. The components $\Delta P_{||}{}^{+-}$ induce the shear waves, which on the Y-sites generate the superplastic behaviour of the grain- rolling type.[12]

Subsurface superheating is established in the basin with dominant $\Delta T_\perp{}^-$ in the presence of ablation, as mentioned previously. Various kinds of craters, bubbles or irregular flow which is combination of $v_\perp$ motion of subsurface liquid to the surface, and $v_{||}$ i.e. flow on the surface may also be observed.[8]

Surface glazing is established in the basins in which maximal temperature $T_S > T_M$. A very fast quenching to the room temperature, associated with the strong surface tension γ, makes the frozen surface smooth, and of the amorphous structure.

2D turbulent flow is established in the basins $T_S > T_M$ with dominant $\Delta T_{||}$ and $\Delta P_{||}$ components, which induce the $v_{||}$ shear flow, with the Rayleigh number $Ra = \frac{v_{||}\, d}{\nu}$ (d = basin size, ν = kinematic viscosity) which can take a large scale of the Ra values. Various kinds of turbulent patterns are generated on 10 ns τ-scale on Ta surface with Nd:YAP laser-spanning the range of purely periodic vortex-type patterns, to the merged-vortex pairs of ∞ type, elongated and finally purely chaotic ones. At the basin boundaries they show tenderadency to stratification.[17]

Thermal convection instability is established in the basin with $T_S > T_M$. Dominant role has the thermal gradient component $\Delta T_\perp{}^+$ which generates vertical convection velocity $v_\perp$. The convection appears for the Rayleigh number $Ra = \frac{v_{||}\, d}{\nu}$ (d = surface layer thickness) equal or higher than 10^3.

Rayleigh-Taylor instability is established in the basin with $T_S > T_B$. Dominant role has the thermal gradient component $\Delta T_\perp{}^+$ which induces a vertical gradient density $\Delta\rho_\perp$. It is responsible for appearance of two layer system of low density ρ_L and the high density ρ_H. Vertical pressure gradient component $\Delta P_\perp{}^+$ pushes the low density layer into the lower high density one, thus generating the R-T instability, which appears for the Atwood number $A = \frac{\rho_H - \rho_L}{\rho_L + \rho_H} \approx 1$.[16]

The arise of various phenomena is derived from various configurations of the first-directional derivation of the T and P stochastic fields. In the second approximation every basin may be distinguished with respect to the dominant component of the material parameters, and consequently with respect to the symmetry of related kinetic coefficients. This would lead to the basin division into subbasins. Obviously, this division would not give a new classes of phenomena, but the pattern structure (geometric and topological characteristic) as a different subclasses of the same phenomena (different pattern symmetries).

This is a necessary step to study of dynamics on the basis of various models (linear and nonlinear) in the particular basin.

Conclusion

We considered inhomogeneity in the L-M interaction which manifests as a number of localized physical processes (phenomena), simultaneously taking place in the interaction space. The concept of inhomogeneity discussed here is based on the beam related reasons.

The stochastic optical field establishes the stochastic field in the interaction space, which initiate various kinds of (stochastic) processes. The interaction space is devided in to the isolated domains and subdomains (basins) of the characteristic, localized response. Various classes of dissipative, dynamics processes may simultaneously appear in these basins existing in the close vicinity.

This problem is of a complex nature; it has a few complexity levels represented by the hierarchical tree introduced previously.[1] The concept of domains and subdomains (basins) represented by different combinations of ΔT and ΔP gradient components is a valuable one, since it includes a great deal of phenomena really observed in the experiments or in the technological processes. On this basis a number of inhomogeneous patterns observed in laser technological applications may be understood, classified, or possibly modified according to the requirements. Further development of the concept requires a more basic treatment and the exact mathematical approach, which to our knowledge was not yet done.

References

1. S. Lugomer; Vacuum; 43 (1992) 1217.

2. F.T. Arecchi; Physica; D51 (1991) 450.

3. E.J. D'Angelo, C. Green, J.R. Fredicce, N.B. Abraham, S. Balle, Z. Chen and G.L. Oppo; Physica; D61 (1992) 6.

4. F.T. Arecchi, S. Boccaletti, G. Giacomelli, G.P. Pucioni, P.L. Kamazza and S. Residori; Physica; D61 (1992) 25.

5. B. Luk'yanchuk; Modeling of Pulsed-laser Ablation and Surface Instabilities; ISLOE'93, Singapore, 11-13, Nov 1993.

6. M.E. Ashby and K.E. Earterling; Acta Metall., 32 (1984) 1935.

7. Phasor; A rotating line used to represent a sinusoidally varying quantity. The length of the line represents the magnitude of the quantity, and its angle with the x-axis at any instant represents the phase.

8. D. Bhattacharya, R.K. Singh and P.H. Holloway; J. Appl. Phys., 70 (1991) 5433.

9. S. Lugomer, M. Stipančić and M. Kerenović; Vacuum; (in press).

10. S. Lugomer; Vacuum; 44 (1993) 1053.

11. C.T. Walters and A.H. Clauer; Appl. Phys. Lett., 36 (1978) 713.

12. S. Lugomer, K. Furić, M. Stipančić and R. Ročak; "Grain-Rolling Superplasticity Induced by Q-Switched Nd:YAG Laser on Tungsten Surface; ISLOE'93, Singapore, 11-13 Nov. 1993.

13. S. Lugomer, G. Bitelli and M. Stipančić; "Laser-Hardening of Tantalum in the Nitrogen Atmosphere", ISLOE'93, Singapore, 11-13 Nov. 1993.

14. S. Lugomer, G. Bitelli and M. Stipančić; "The CO2 Laser Effects on Metal Surface", Technical Report on Cooperation between "Ruđer Bošković" Institute and ENEA INN. SVIL. Frascatii, to be published by Frascati Center, Roma, Italy (1993).

15. E. Bodenschatz, D.S. Connell, J.R. de Brugu, R. Ecke, Y.C. Hu, K. Lerman and G. Ahlers; Physica; D61 (1992) 77.

16. S. Lugomer and M. Stubičar; Vacuum (in press).

17. S. Lugomer, M. Stipančić and J. Kvapil; (Results of Cooperation between "Ruđer Bošković" Institute Zagreb and "Monokrystali" Laser Factory, Turnov, The Czech Republic) unpublished.

Prispelo (Arrived): 09.12.93 *Sprejeto (Accepted): 10.03.94*

Dr. S. Lugomer, dipl. ing.
Institut Ruđer Bošković
Bijenička 54
41000 Zagreb
tel. +85-41-45 111
fax. +385-41-425 497